Publisher: Engineering College, Al Muthanna University

Open Access

DOI:10.52113/3/eng/mjet/2025-13-03-/27-33, Vol. (13), Issue (3), (2025)

Muthanna Journal of Engineering and Technology MJET

Submitted 30 June 2025, Accepted 29 August 2025, Published online 03 October 2025

Seed Detection algorithm using multi-thresholding measures on histopathological images

Salah Alheejawi[a], Ruwaidah F. Albadr[b], Ahmed Saaudi[c] , Osamah Thamer Hassan Al-zubaidi[d]

[ab]ICT Department, Technical Institute of Samawah, Al-Furat Al-Awsat Technical University, Al-Muthanna, Iraq.
[c]Electronics and Communication Engineering, Al Muthanna University, Samawah, Iraq
[d]Department of Prosthetics and Orthotics Engineering, University of Kerbala, Kerbala, Iraq.
**Corresponding author E-mail: ahmed.saaudi@mu.edu.iq*

Abstract

The recent advancing of computational resources, led to a significant improvement in histopathological image analysis. These improvements helped to diagnosis various diseases and dive into cellular level of the tissue for accurate prognosis. Therefore, an automated algorithm is proposed to enhance diagnostic accuracy and efficiency. This paper proposes a detection technique to detect the cells nuclei on histopathological images that are stained by Hematoxylin and Eosin (H&E). The proposed technique applies multiple thresholds on the grayscale image version of the H&E-stained image and from each resulted binary image, several centroids are extracted for each disconnected foreground region. Three measures such as area, centroid location, and circularity ratio have been used to determine the selection of nuclei seed. The technique assigns certainty weights based on threshold values, enhancing the reliability of detected seeds. Comparisons with existing methods, like the generalized Laplacian of Gaussian (gLoG) technique, demonstrate the proposed method's efficiency and accuracy, providing a robust foundation for further segmentation processes.

Keywords: Histopathological Images; H&E-Stained Images; Multi-Thresholding; Nuclei Segmentation; Seed Detection

1. Introduction

Histopathological images, obtained through the microscopic examination of tissue samples, play a critical role in the diagnosis and study of diseases such as cancer. These images provide detailed visual information about the cellular and tissue structure, enabling pathologists to identify abnormalities and disease states. The significance of histopathological images lies in their ability to reveal the morphological characteristics of cells, which are essential for accurate diagnosis, prognosis, and treatment planning. However, the manual analysis of these images is time-consuming, labor-intensive, and prone to inter-observer variability, highlighting the need for automated image processing techniques to assist pathologists and improve diagnostic accuracy [1,2].

The main challenge in automated techniques that analysis histopathological images directly is the identification and segmentation of nuclei in the tissue. The cell nuclei is the most important element in the tissue, where the morphological features can be used to define and classify various of cells, and separate them from malignant cells [3,4]. The nuclei segmentation can be difficult due the variations of cell in shape, color, size, and staining intensity, as well as the presence of overlapping nuclei and artifacts in the images. To overcome these issues, different nuclei segmentation algorithms have been

proposed in the literature [5,6]. Most of these algorithms, use a detection of nuclei technique, as a first step, followed by nuclei segmentation process

In the literature, seed detection techniques are a powerful step that can identify cell centers, utilized as starting points for more comprehensive segmentation methods. Detecting the cell seeds accurately can be crucial, with traditional method, especially when the cells loose the blob shape. In [7], restricted randomized Hough transform is used, to accurately detect ellipse shapes on the histopathology images. In [8], an automated seed detection is used to count the cytotoxic T-cells in CD-8 stained renal biopsy images. The study introduces a method that employs a multi-scale difference of Gaussian technique to identify potential T-cells regions in both color and intensity channels of immunostained images. The integration of data from these channels enhances the accuracy of cell detection, significantly reducing the time and effort required for manual counting. In [9], a novel approach is presented for the automatic detection and segmentation by combining advanced techniques like graph-cuts-based binarization, multiscale Laplacian-of-Gaussian filtering, and adaptive scale selection to enhance accuracy and efficiency. In [10,11], the authors presents a method for detecting seed nuclei in histopathology images using Generalized Laplacian of Gaussian filters to enhance detection accuracy. The technique consist of several steps such as preprocessing, filtering, segmentation, and post-processing to achieve high accuracy and robustness in nuclei detection [12-16].

The proposed seed detection consists of the following steps. Firstly, convert the input Hematoxylin and Eosin (H&E)-stained image into a grayscale image. Secondly, determine the potential nuclei regions by applying multiple thresholds to generate multiple binary images to define centroids of ROIs in each binary image. Finally, perform further feature analysis defined by area, centroid location, and circularity ratio to determine the seeds accurately. The experimental results show that the proposed method is an efficient and adaptable solution for nuclei detection in histopathological images in terms of computational complexity and detection accuracy.

2. Proposed Technique

Seed detection is an important step for many nuclei segmentation techniques. In this section, we propose a technique to detect the nuclei seeds in an H&E-stained image of skin tissue. The technique is implemented by applying multiple thresholds on the gray scale image. The seed detection process is explained in the following:

1. The input H&E-stained image is converted into a gray level image. Let the gray level image be denoted by G.
2. A number of thresholds (K) are applied on the image G to obtain K binary images B_i ($i = 0,1,...,K-1$). The threshold values, denoted by T_i, are between T_0 and T_{K-1}. In this paper, $T_0 = 0.25$ and $T_{K-1} = 0.80$. The values of the thresholds are selected as: $T_i = T_0 + 0.05i$.

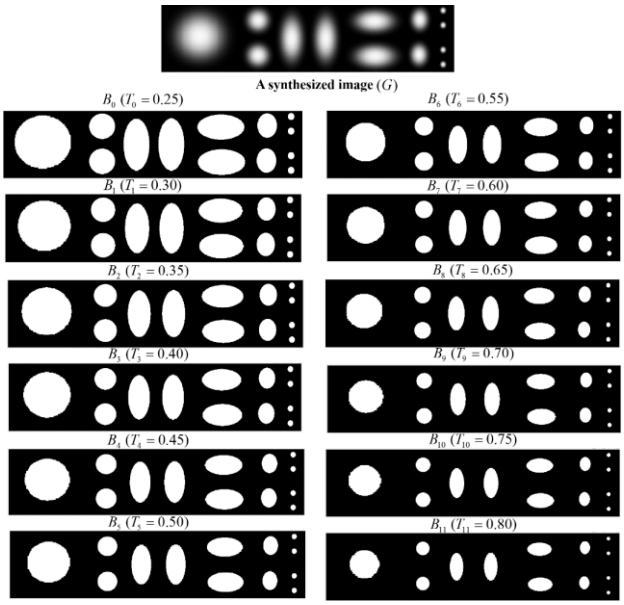

Fig.1. A gray level image G and the obtained binary masks (i.e., foreground regions) B_i. The mask B_i is obtained by applying threshold T_i.

Fig.1 shows a synthesized image *G* (in the top row) with 13 objects of different shapes and sizes. The objects have 2D gaussian shapes with different σ_x and σ_y values. The next six rows show the binary images B_i obtained by applying 12 different thresholds (*K*=12) on the image *G*. Each binary image B_i includes several disconnected foreground regions. Let the number of the disconnected regions be denoted by *R*. In Fig. 1, *R*=13 for all B_i. Note that the size of the (disconnected) foreground (or mask) regions in B_i's vary with i as different thresholds T_i are used to obtain these images.

3. For each of the *R* foreground regions (FR) in a B_i, three features: area (A), centroid location (L), and circularity ratio (C) are calculated. Note that *A* equals to the number of pixels in the FR, *L* is the centroid of the FR, and the circularity ratio C of an FR is calculated as follows:

$$C = \frac{4\pi A}{P^2} \tag{1}$$

where *P* is the perimeter of the FR.

4. In order to detect the seeds, we generate clusters of centroids *L* corresponding to all FRs from all B_i. A Mean Shift technique is applied on the locations *L* of the *K* binary images to generate clusters. Let the number of the detected clusters be denoted by *P* (in an ideal case, *M* should be same as the number of objects in the image). Denote the obtained centroid clusters by C^P (*p*=1,2,..,*P*). The number of centroids (L) in the cluster *m* can vary, and let it be denoted by N_m. An example of the clustering is shown in Fig. 2(b) where *M* = 13 and $N_m = 12$ for all *m*.

The top row of Fig.2 (b) shows the overlapped boundaries of the FR's that are obtained from all B_i -the inner and outer boundaries are obtained using the highest and lowest thresholds, respectively. Note that for each object in Fig. 2(a), there are 12 superimposed boundaries as well as 12 superimposed centroids (some of these centroids are shown with red bounding squares). The green rectangular region in Fig.2 (b) shows the boundaries of superimposed masks B_i. In Fig.2 (b) bottom row, a blown-up version of these (7) red squares are shown. It is observed that each centroid cluster has 12 centroids shown with different color dots.

5. The FR's obtained with larger threshold values are likely to be more conservative estimate of the segmented masks. Therefore, higher weights may be assigned to these mask estimates. In this work, certainty weights (Cw) are assigned to the center location (*L*) of the FR's depending on the threshold values used. Assume that the predetermined range of the Cw is $[W_{\min}, W_{\max}]$. The Cw for threshold T_i is calculated as follows:

$$Cw_i = \beta(T_i - T_0) + W_{\min} \tag{2}$$

where $\beta = \dfrac{W_{\max} - W_{\min}}{T_{K-1} - T_0}$

In this work, $W_{\min} = 0.1, W_{\max} = 1$. With $T_0 = 0.25$ and $T_{K-1} = 0.80$, β is obtained as 1.63.

6. For each of the *M* clusters, three parameters: certainty measure (CM), circularity measure (CrM), and size measure (SM) are calculated. For *p*th cluster, these parameters are calculated as follows:

$$\begin{aligned} M_C^p &= \sum_{n=1}^{N_p} Cw_n \\ M_{Cr}^p &= \sum_{n=1}^{N_p} C_n \\ M_S^p &= \sum_{n=1}^{N_p} S_n \end{aligned} \tag{3}$$

Although ideally the clusters should have Note that the clusters may have different numbers of (L).

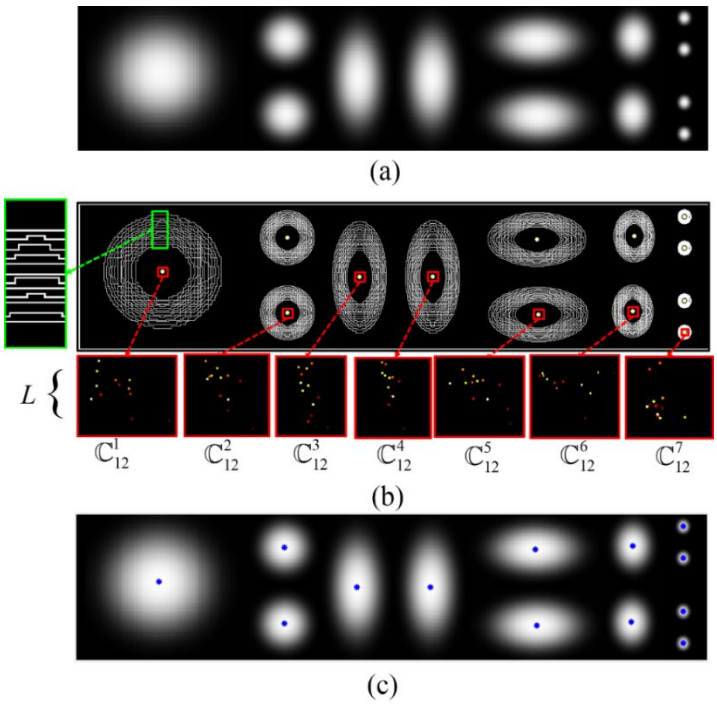

Fig. 2. An example of the proposed Seed Detection process (a) a synthesized image, (b) intermediate results (c) Seed detection results.

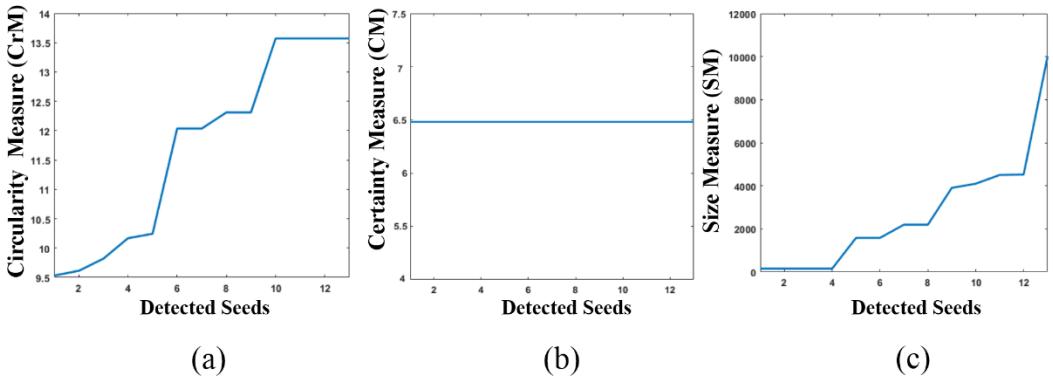

Fig.3 An example of calculated measures for the synthesized image in Fig.1 (a) Circularity measure, (b) Certainty measure (c) Size measure.

Fig.2 shows the calculated measures of the synthesized image in Fig. 1 for 13 detected seeds. Fig.2 (a) represents the circularity measures (CrMs) of all the detected seeds, and it is observed there are 4 have around 13.5 CrM belonged to last small four gaussian on the synthesized image in Fig. 1.

Fig.2 (b) shows the certainty measure of the detected seeds, and it is observed that all seeds have assigned with same certainty measure because each seed cluster having same number of centers. In Fig. 2 (c) the size measure is represented for all the detected cells, and it is calculated based on the size of a white disconnected region after each threshold. In each cluster will have multiple sizes and the minimum value is chosen for presenting the size of that cluster.

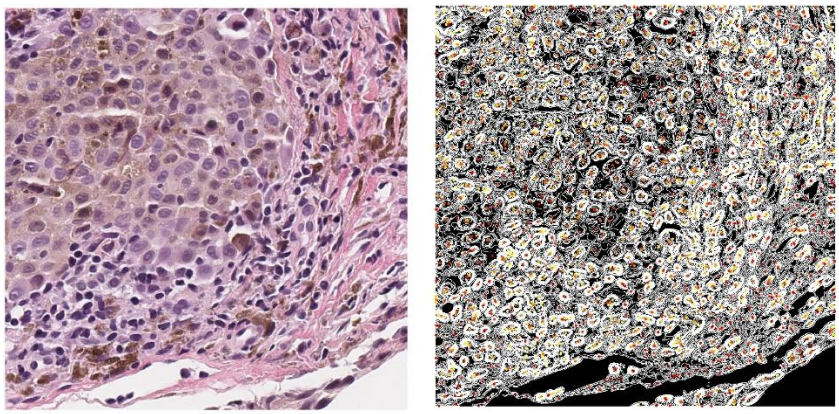

(a) (b)

Fig. 4. Seed Detection results (a) H&E-stained image, (b) intermediate results, where heat colors shades show the certainty of the detected seed.

3. Results

In this section, we present the subjective comparison between the proposed technique and gLoG technique. Fig. 3, shows the detection results of the proposed technique results in (a) and the gLoG technique results in (b). The gLoG technique has many disadvantages over the proposed technique including the complexity introduced by number of convolutional operations and un-generalized parameters defined with values of σ_x , and σ_y .

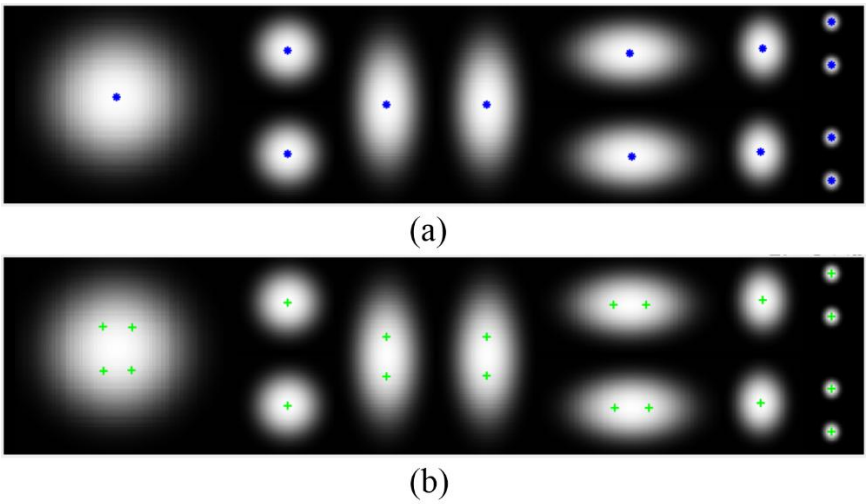

(a)

(b)

Fig.5 Subjective comparison of Seed detection techniques applied on the synthesized image in Fig.1 (a) proposed technique, (b) gLoG technique.

Let GT, DS and TP denote the numbers of ground truth seeds, detected seeds and true positives seeds, respectively. The performance is evaluated with respect to the recall, precision and F-measure which are defined as follows:

$$Recall = \frac{TP}{GT} \times 100\%$$

$$Precision = \frac{TP}{DS} \times 100\%$$

$$F - score = \frac{2 \times (Precision \times Recall)}{Precision + Recall} \times 100\%$$

Table 1 The seed detection performance.

Techniques	recall	precision	F-Score
RRHT [7]	72.97	85.94	78.89
DoG [8]	83.05	80.20	81.53

mLoG [9]	88.67	87.08	87.83
gLoG [11]	89.45	94.20	91.72
Proposed technique	97.39	95.45	93.33

Table 1 The seed detection performance.

Techniques	recall	precision	F-Score
RRHT [7]	72.97	85.94	78.89
DoG [8]	83.05	80.20	81.53
mLoG [9]	88.67	87.08	87.83
gLoG [11]	89.45	94.20	91.72
Proposed technique	97.39	95.45	93.33

4. Conclusion

The accurate detection of nuclei seeds is a critical step in the segmentation of histopathological images, significantly impacting the diagnosis and treatment of diseases such as cancer. The proposed seed detection algorithm, which employs a multi-threshold approach on grayscale images followed by centroid clustering, offers a reliable and efficient solution for nuclei segmentation. By calculating and utilizing features like area, centroid location, and circularity ratio, and assigning certainty weights to detected seeds, the method ensures high accuracy in identifying true nuclei regions. Subjective comparisons with existing techniques, such as the gLoG method, highlight the proposed algorithm's advantages in terms of computational efficiency and parameter generalization. This work underscores the potential of advanced image processing techniques in enhancing diagnostic capabilities and supports the ongoing development of automated tools for histopathological analysis. Future research may focus on further optimizing the algorithm and exploring its applicability to a broader range of histopathological datasets.

References

[1] Kumar, N., Verma, R., Sharma, S., Bhargava, S., & Lal, R. (2017). A review on image processing techniques for nuclei detection and classification in histopathological images. Biomedical Signal Processing and Control, 34, 17-30.
[2] Xing, F., & Yang, L. (2016). Robust nucleus/cell detection and segmentation in digital pathology and microscopy images: a comprehensive review. IEEE reviews in biomedical engineering, 9, 234-263.
[3] Ronneberger, O., Fischer, P., & Brox, T. (2015). U-Net: Convolutional networks for biomedical image segmentation. In International Conference on Medical image computing and computer-assisted intervention (pp. 234-241). Springer, Cham.
[4] Comaniciu, D., & Meer, P. (2002). Mean shift: A robust approach toward feature space analysis. IEEE Transactions on Pattern Analysis and Machine Intelligence, 24(5), 603-619.
[5] Cheng, Y., Zhou, X., & Xu, J. (2017). Automated segmentation of cell nuclei in histopathology images. Biomedical Optics Express, 8(10), 5146-5159.
[6] Fernandez-Gonzalez, R., & Willis, M. (2018). Automated nuclei segmentation using the Laplacian of Gaussian and region growing algorithms. Journal of Pathology Informatics, 9, 27.
[7] Kumar, N., Verma, R., Sharma, S., Bhargava, S., & Lal, R. (2017). A review on image processing techniques for nuclei detection and classification in histopathological images. Biomedical Signal Processing and Control, 34, 17-30.
[8] Xing, F., & Yang, L. (2016). Robust nucleus/cell detection and segmentation in digital pathology and microscopy images: a comprehensive review. IEEE reviews in biomedical engineering, 9, 234-263.
[9] Ronneberger, O., Fischer, P., & Brox, T. (2015). U-Net: Convolutional networks for biomedical image segmentation. In International Conference on Medical image computing and computer-assisted intervention (pp. 234-241). Springer, Cham.
[10] Comaniciu, D., & Meer, P. (2002). Mean shift: A robust approach toward feature space analysis. IEEE Transactions on Pattern Analysis and Machine Intelligence, 24(5), 603-619.
[11] Cheng, Y., Zhou, X., & Xu, J. (2017). Automated segmentation of cell nuclei in histopathology images. Biomedical Optics Express, 8(10), 5146-5159.
[12] Fernandez-Gonzalez, R., & Willis, M. (2018). Automated nuclei segmentation using the Laplacian of Gaussian and region growing algorithms. Journal of Pathology Informatics, 9, 27.
[13] Cheng, Z., & Liu, Y. (2004). Efficient technique for ellipse detection using restricted randomized Hough transform. In *Proceedings of International Conference on Information Technology: Coding and Computing* (Vol. 2, pp. 714–718). IEEE.
[14] Niazi, M. K. K., Satoskar, A. A., & Gurcan, M. N. (2013). An automated method for counting cytotoxic T-cells from CD8 stained images of renal biopsies. In *SPIE Medical Imaging* (pp. 867606–867606). International Society for Optics and Photonics.
[15] Al-Kofahi, Y., Lassoued, W., Lee, W., & Roysam, B. (2010). Improved automatic detection and segmentation of cell nuclei in histopathology images. *IEEE Transactions on Biomedical Engineering*, 57(4), 841–852.
[16] Kong, H., Akakin, H. C., & Sarma, S. E. (2013). A generalized Laplacian of Gaussian filter for blob detection and its applications. *IEEE Transactions on Cybernetics*, 43(6), 1719–1733.
[17] Xu, H., Lu, C., Berendt, R., Jha, N., & Mandal, M. (2017). Automatic nuclei detection based on generalized Laplacian of Gaussian filters. *IEEE Journal of Biomedical and Health Informatics*, 21(3), 826–837. doi: 10.1109/JBHI.2016.2544245.

[18] Balasubramanian, A. A., Al-Heejawi, S. M. A., Singh, A., Breggia, A., Ahmad, B., Christman, R., Ryan, S. T., & Amal, S. (2024). Ensemble Deep Learning-Based Image Classification for Breast Cancer Subtype and Invasiveness Diagnosis from Whole Slide Image Histopathology. Cancers, 16(12), 2222. https://doi.org/10.3390/cancers16122222.

[19] Alheejawi, S., Berendt, R., Jha, N., Maity, S. P., & Mandal, M. (2021). An efficient CNN based algorithm for detecting melanoma cancer regions in H&E-stained images. 2021 43rd Annual International Conference of the IEEE Engineering in Medicine & Biology Society (EMBC), 3982-3985. https://doi.org/10.1109/EMBC46164.2021.9630443.

[20] Alheejawi, S., Berendt, R., Jha, N., & Mandal, M. Melanoma Cell Detection in Lymph Nodes Histopathological Images using Deep Learning (2020). Signal & Image Processing: An International Journal (SIPIJ) Vol.11, No.4, August 2020, Available at SSRN: https://ssrn.com/abstract=3693658.

[21] Jain, M. N., Al-Heejawi, S. M. A., Azzi, J. R., & Amal, S. (2025). Digital Pathology and Ensemble Deep Learning for Kidney Cancer Diagnosis: Dartmouth Kidney Cancer Histology Dataset. Applied Biosciences, 4(1), 8. https://doi.org/10.3390/applbiosci4010008

[22] Mudavadkar, G. R., Deng, M., Al-Heejawi, S. M. A., Arora, I. H., Breggia, A., Ahmad, B., Christman, R., Ryan, S. T., & Amal, S. (2024). Gastric Cancer Detection with Ensemble Learning on Digital Pathology: Use Case of Gastric Cancer on GasHisSDB Dataset. Diagnostics, 14(16), 1746. https://doi.org/10.3390/diagnostics14161746